Available online at www.sciencedirect.com
ScienceDirect
Journal of Structural Biology 161 (2008) 120–132
Journal of Structural Biology
www.elsevier.com/locate/yjsbi

Influence of microstructure on deformation anisotropy of mineralized cuticle from the lobster *Homarus americanus*

C. Sachs, H. Fabritius *, D. Raabe

Max-Planck-Institut für Eisenforschung, Max-Planck-Strasse 1, 40237 Düsseldorf, Germany

Received 5 July 2007; received in revised form 27 September 2007; accepted 29 September 2007
Available online 10 October 2007

Abstract

The exoskeleton of the American lobster *Homarus americanus* is a hierarchically organized nano-composite material consisting of organic chitin–protein fibers associated with inorganic calcium carbonate. The presence of a well-developed and periodically arranged pore canal system leads to a honeycomb-like structure. The concomitant presence of the twisted plywood arrangement of the mineralized chitin–protein fibers alters the elastic properties, the deformation behavior, and fracture behavior compared to classical honeycomb structures. By performing compression tests in various directions of the cuticle we examined the anisotropic elastic–plastic deformation and fracture behavior of mineralized parts of the exoskeleton. By applying digital image correlation during compression testing, the evolution of the elastic–plastic deformation at the microscopic scale was observed with high resolution and simultaneously global stress and strain data were acquired. Shear tests were performed in order to determine the fracture energy for different shear planes and directions. The investigation of the microstructure after plastic deformation revealed the underlying deformation mechanisms of lobster endocuticle from the claws under different loading conditions. For evaluating the effect of hydration the samples were tested both in the dry and in the wet state.

Keywords: Mechanical properties; Fracture behavior; Anisotropy; Arthropod cuticle

1. Introduction

Biological materials often combine various mechanical principles of construction and are simultaneously multifunctional according to the requirements of the organism. A major design principle in nature is the hierarchical organization which is perfectly implemented in the exoskeletons of Arthropoda (Vincent and Wegst, 2004) or other mechanically relevant structures like the bones of vertebrates and the shells of mollusks. The exoskeleton is formed by the cuticle of arthropods and consists of chitin and various proteins. Most members of the Crustacea, which represent an important group inside the Arthropoda, implement variable amounts of nanoscopic crystalline or amorphous calcium carbonate particles to harden the exoskeleton in the rigid body parts like the chelipeds in contrast to the flexible parts like joint membranes (Roer and Dillaman, 1984). The American lobster *Homarus americanus* is a large sized crustacean. Its body can be divided into the head (cephalon), the thorax, and the tail (abdomen). The first three pairs of walking legs which are attached to the thorax end in true pincers (Factor, 1995). Characteristically, the first pair is enlarged to massive and flattened claws which are referred to as crusher claw and pincher claw according to their biological function (Travis, 1963; Vernberg and Vernberg, 1983). Arthropod cuticle consists of the apical epicuticle and the inner procuticle (Hadley, 1986). While the epicuticle as thin waxy layer provides a permeability barrier to the environment, the procuticle which can be subdivided into the exocuticle and the endocuticle is the mechanically relevant layer. Both sublayers are made up of mineralized chitin–protein fibers

* Corresponding author.
E-mail addresses: c.sachs@mpie.de (C. Sachs), h.fabritius@mpie.de (H. Fabritius), d.raabe@mpie.de (D. Raabe).

1047-8477/$ - see front matter © 2007 Elsevier Inc. All rights reserved.
doi:10.1016/j.jsb.2007.09.022

forming a twisted plywood structure with different rotation angles, which leads to different lamella thicknesses in the exo- and the endocuticle (Giraud-Guille, 1998). Due to the mechanical loads occurring in the two claws, particularly the thickness of the endocuticle is strongly increased to the millimeter range whereas the thickness of the exocuticle remains constant at values of about 200 μm. Epi- and procuticle represent the highest level in the hierarchical organization of the lobster's exoskeleton (Fig. 1a, I). The next lower level is the twisted plywood- or Bouligand structure (Fig. 1a, II and b) which is formed by stacking planes of parallel arranged mineralized chitin–protein fibers (Fig. 1a, III) and rotating them around the normal axis of the cuticle (Bouligand, 1970; Giraud-Guille, 1984; Weiner and Addadi, 1997). The distance in which a rotation of 180° is completed can be defined as the stacking height of the twisted plywood structure (Fig. 1b). The mineralized chitin–protein fibers (Fig. 1a, IV) have diameters between 50 and 250 nm and consist of clustered chitin–protein nanofibrils interspersed with nanoscopic particles of amorphous or crystalline calcium carbonate. The nanofibrils themselves are α-chitin crystals wrapped in proteins (Fig. 1a, V) with diameters of about 2–5 nm and lengths of about 300 nm. They contain 18–25 chains (Fig. 1a, VI) of chitin molecules (Fig. 1a, VII) arranged in an anti-parallel fashion (Giraud-Guille, 1990; Andersen, 1999). Besides the twisted plywood structure a second design principle can be found in the lobster cuticle. Due to a well-developed pore canal system a honeycomb-like structure is generated as numerous canals penetrate the cuticle perpendicular to its surface (Fig. 1b and c). Each pore canal contains a long, soft, and probably flexible tube which has an elliptical-like outline with the long axis of the ellipse parallel to the fiber orientation in each plane (Fig. 1c). Due to the rotation of the twisted plywood structure the outer shape of each tube resembles a twisted ribbon. Similar pore canals are also present in the cuticle of crabs like *Carcinus maenas* (Compère and Goffinet, 1987).

The combination of a honeycomb-like structure and a twisted plywood structure with tightly connected lamellae should lead to remarkable mechanical properties (Sachs et al., 2006a) and an anisotropic deformation behavior. To investigate the elastic–plastic deformation behavior and its anisotropy at a global and a local scale we performed compression tests combined with digital image correlation (Sachs et al., 2006b) as well as shear tests on endocuticle samples extracted from the claws. A detailed analysis of the deformed microstructure revealed the underlying deformation mechanisms in the examined cuticle parts of the lobster *H. americanus*.

2. Materials and methods

2.1. Sample preparation

The specimens used for compression and shear tests were taken from the chelipeds of two large adult, non-molting American lobsters (*H. americanus*) bought from a local

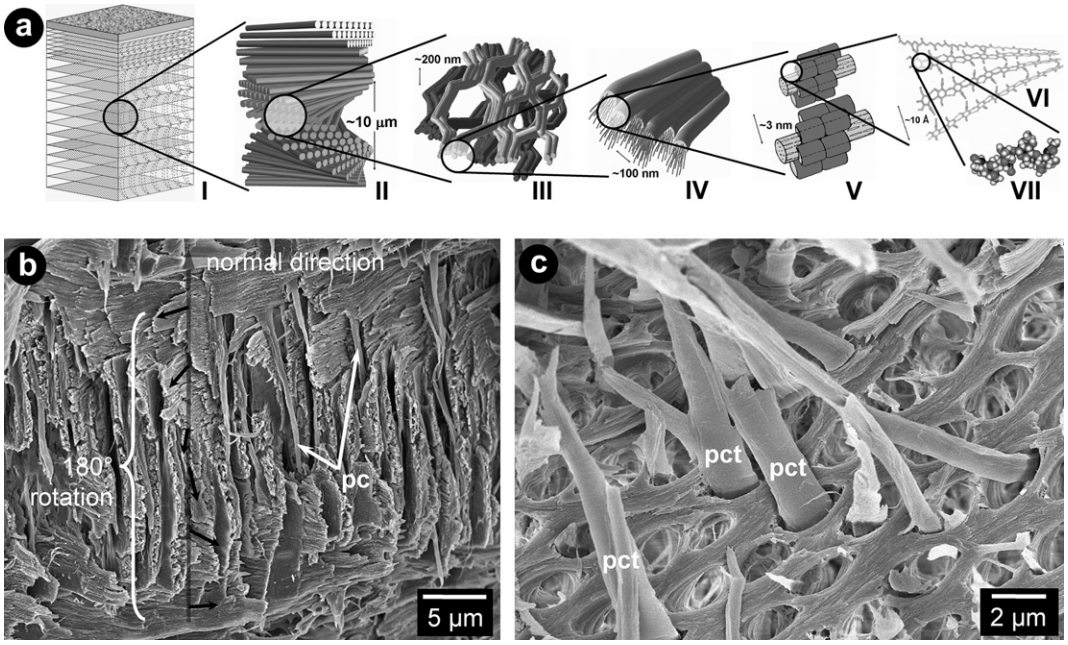

Fig. 1. Microstructure of lobster cuticle. (a) Schematic depiction of the hierarchical organization from the macro- to the nanoscale: the three layered cuticle (I) with its twisted plywood arrangement (II) of superimposed planes of parallel chitin–protein fibers arranged around the cavities of the pore canal system (III). The chitin–protein fibers (IV) consist of bundled nanofibrils (V) containing protein wrapped anti-parallel α-chitin chains (VI) which themselves are build of *N*-acetyl-glucosamine molecules (VII). (b) Cross fracture of air-dried endocuticle showing a 180° rotation of superimposed fiber layers around the normal direction (black arrows) with interspersed perpendicular pore canals (pc). (c) The typical honeycomb-like structure resulting from the extremely well-developed pore canal system observed in endocuticle fractured parallel to the surface. The long and probably flexible pore canal tubes (pct) are preserved in many of the pore canals.

food supplier. Two sets of samples were dissected from the pincher and the crusher claws of both specimens. One set was air-dried while the other one was stored at low temperatures in a humid atmosphere (4 °C, >90% RH) in order to prevent desiccation. Exposure of these samples to ambient conditions during preparation and testing was kept to a minimum.

All test specimens were manufactured using a compact i-mes CPM 4030 CNC milling machine (i-mes GmBH, 36132 Eiterfeld, Germany). For the compression tests 18 dry and 18 wet cuticle pieces were milled to tetragonal test specimens with a height of 3 mm and a side length of 2 mm (Fig. 2b). To account for the anisotropy of the material, they were prepared considering two distinct orientations with respect to the geometry and microstructure of the cuticle. Six test specimens were machined with their long edge oriented parallel to the normal direction of the cuticle for compression in normal direction, both in dry and in wet condition. The other 12 test specimens were machined with their long edge oriented perpendicular to the normal direction of the cuticle for compression in transverse direction, both in dry and in wet condition. Due to the machining process the exocuticle was removed and thus all test specimens consist solely of endocuticle. Before the compression tests the white sample surfaces were decorated with a graphite aerosol spray to create a stochastic black spot pattern for better contrast as required for digital image correlation. During testing the wet samples were exposed to ambient air without applying any moistening. Afterwards the test specimens used for compression testing were air-dried and prepared for electron microscopy. The test specimens were cleaved and the fracture surfaces were sputter-coated with 10 nm gold, mounted on aluminum sample holders and examined in a CamScan 4 scanning electron microscope.

For the shear tests nine dry cuticle pieces were milled to tetragonal test specimens with a height of 5 mm and a side length of 2 mm. Three test specimens were machined with their long edge oriented parallel to the normal direction of the cuticle and six test specimens with their long edge oriented perpendicular to the normal direction of the cuticle. Like the compression test samples, the test specimens consisted solely of endocuticle. The shear tests were performed without using digital image correlation.

2.2. Compression tests and digital image correlation

The compression tests were performed on a special miniaturized tensile test rack by Kammrath & Weiss GmbH (44141 Dortmund, Germany). The computerized device features two moveable crossheads allowing the sample to remain in a stable centered position during testing (Fig. 2a). The faces of cylindrical dies were polished to minimize friction between their surface and the test specimens (Fig. 2b). The maximum capacity of the load cell (Precision force transducer ALM 170) was 1000 N with an error of 0.3% at room temperature. The elongation speed amounted to 6.0 μm/s which translates to a strain rate of $2 \times 10^{-3}\ s^{-1}$.

In order to record the deformation during the compression tests, two digital cameras mounted perpendicular to the tensile test rack were used for taking images enabling the three-dimensional localization of each point on the sample surface (Fig. 2a). The cameras (CCD-1300: VDS Vosskühler GmbH, 49084 Osnabrück, Germany) feature a resolution of up to 1300 dpi and were equipped with lenses of 50 mm focal length and a maximum aperture of 2.8 (Schneider-Kreuznach, 55543 Bad Kreuznach, Germany). The camera set-up is controlled by the ARAMIS system (GOM—Gesellschaft für Optische Messtechnik mbH, 38106 Braunschweig, Germany). Digital pictures were recorded every 1 s which corresponds to an elongation of 6 μm.

The post-processing of the sets of digital images was performed following the procedure described in detail in an earlier study on the elastic–plastic deformation of lobster cuticle (Sachs et al., 2006a). The digital image correlation (DIC) was performed using the ARAMIS software version V6.0.0-3 (GOM—Gesellschaft für Optische Messtechnik mbH). The decoration with graphite aerosol applied to the sample surfaces before loading was used as input pattern for the recognition of geometrical changes in the gray scale distribution. In order to evaluate the quality of the stochastic pattern we recorded two images of every sample before deformation and compared the calculated strain maps. If the observed intrinsic noise was more than 0.01%, the sample was not used for compression testing. These images were also used to ensure that the samples were properly illuminated and no reflections occurred on

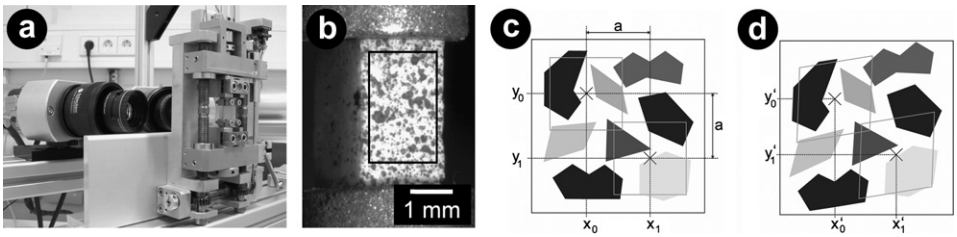

Fig. 2. (a) Test rack equipped with two cameras used for 3D-digital image correlation (DIC). (b) Compression test sample and marked area of interest for DIC (black rectangle). (c and d) Schematic illustration of two single facets used in pattern recognition before (c) and after (d) deformation. Three-dimensional coordinates are assigned to the facet centers before (c; x_0, y_0) and after deformation (d; x_1, y_1). The distance a is the initial step size which defines the spatial resolution (GOM, 2000).

the surface, especially in samples in wet state. A rectangular region of interest (1.6 mm × 2.4 mm) with the same ratio of dimensions like the test specimens was defined on each initial image of the samples (Fig. 2b), leaving margins of 200 μm to the vertical and 300 μm to the horizontal edges in order to eliminate edge-effects in the strain maps. In the selected area a grid of square facets was created. The facet size is defined as the dimension of one single square, the step size "a" as the distance between the centers of two adjacent facets with $a = y_1 - y_0$ or $a = x_1 - x_0$. The facets are characterized by the gray scale distribution and three-dimensional coordinates are assigned to the facet centers before (x_0, y_0) and after deformation (x_1, y_1) (Fig. 2c and d). In this study the facet size was set to a value of 23 pixels corresponding to 219 μm and the step size was set to a value of 10 pixels which is equal to a spatial resolution of 95 μm. In order to obtain strain maps for each sample, the displacement gradient tensor and the resulting strain tensor were computed at each deformation stage. In the final strain maps only the components of strain tensor which represent the local strain in the longitudinal direction ε_y and in the lateral direction ε_x were displayed.

The global (engineering) strain data represent the averaged global strain values derived from the displacement of three pairs of reference points which were defined at both ends of the areas of interest of every test specimen. At a sampling rate of 1 image/s and an elongation speed of 6 μm/s, data points were recorded in global strain intervals of 0.2% and linked to the corresponding stress values. For the determination of Poisson's ratio three additional reference points were defined at both sides of the areas of interest of the test specimens. Poisson's ratio v was determined in the linear elastic region of the stress–strain curves using a strain interval up to 0.5% (Fig. 5). For the evaluation of the structural stiffness the same interval was selected to linearly fit the stress–strain curves. The yield strain ε_y and the yield stress σ_y were derived from the intercept point of the stress–strain curve with a straight line which is shifted 0.01% parallel to the linear part of the curve. The strain at densification ε_d and the stress at densification σ_d were estimated by the use of linear curve fitting in and after the plateau region (Fig. 5). The reliability of the mechanical data obtained by DIC was examined by performing cyclic compression and tensile testing with commercially available polycarbonate (Makrolon®, Bayer MaterialScience AG, Leverkusen, Germany). The obtained values for elastic modulus, Poisson's ratio, yield strength, and yield strain were identical to those obtained by standard testing of standardized samples (DIN EN ISO 10002). The accuracy of the DIC equipment amounts to 0.02% according to the manufacturer.

In order to investigate anisotropy of the elastic–plastic deformation behavior, both dry and wet samples were tested in normal direction of the cuticle (Fig. 3a) and in transverse direction (Fig. 3b and c) of the cuticle. Due to the twisted plywood structure, two observation directions are possible in samples compressed in transverse direction. In the first case the observed sample surface (observation direction I) is parallel to the cuticle surface and represents the in-plane direction of the honeycomb-like structure (Fig. 3b). In the second case the observed sample surface (observation direction II) is the cross section of the cuticle which is equal to the out-of-plane direction of the honeycomb-like structure (Fig. 3c).

2.3. Shear tests

The shear tests were performed using the same experimental equipment used for the compression tests. The compression dies were replaced by special holders which allow clamping tetragonal test specimens (2 mm × 2 mm × 5mm) tautly and displacing both ends in opposite directions. The spacing between the two clamps amounted to about 0.5 mm and the displacement speed was set to 2 μm/s. A total of nine tetragonal test specimens were tested solely in the dry state. Three samples were sheared parallel to the cuticle surface (mode I, Fig. 4a) and six samples were sheared in normal direction of the cuticle whereas the shear plane was either in normal direction (mode II, Fig. 4b) or in transverse direction (mode III, Fig. 4c). The shear tests were conducted without applying digital image correlation.

3. Results

3.1. Compression tests

As the cuticle samples had to be machined to obtain standardized test specimens, the epi- and the exocuticle were removed. Thus, the global stress–strain behavior only reflects the mechanical properties of the endocuticle. The average stress–strain curves obtained from both tested lobsters (*H.a.*1 and *H.a.*2) under compression in normal direction and in transverse direction both in the dry and in the wet state are depicted in Fig. 5.

The samples tested in normal direction display a linear elastic response and deform plastically before fracture. In contrast, the samples tested in transverse direction show

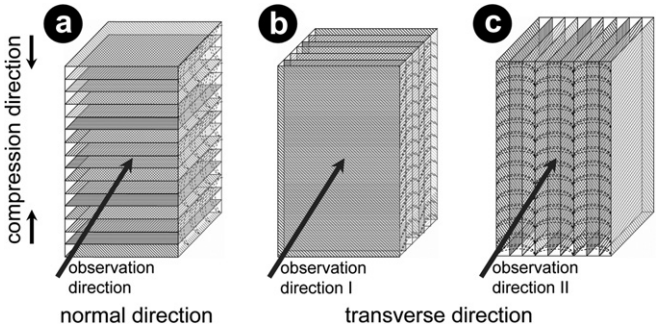

Fig. 3. Schematic figure of the compression testing experiments. (a) Compression applied in normal direction of the cuticle, the cross section is observed. (b and c) Compression applied in transverse direction of the cuticle, the two observation directions are (b) parallel to the surface (I) and (c) the cross section (II).

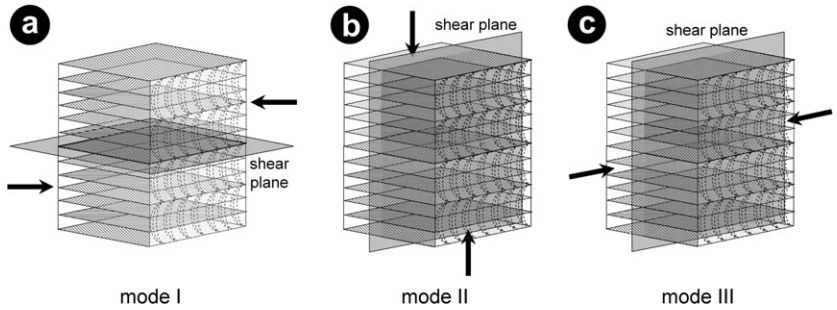

Fig. 4. Schematic figure of the shear tests, arrows indicate the shear direction. (a) In mode I the shear plane is parallel to the cuticle surface. (b) In mode II and (c) III the shear plane is perpendicular to the cuticle surface but the shear direction is either in normal direction (mode II) or in transverse direction (mode III).

a linear elastic regime followed by an extended plateau region and a range of densification before fracture. The characteristics of the stress–strain curves are the same both in the dry and in the wet state. However, the average values for the structural stiffness s_{st}, the yield strain ε_y, the yield stress σ_y, the strain at densification ε_d, the stress at densification σ_d, and the stress to fracture σ_f are higher for the dry samples than for the wet samples with the exception of the strain to fracture ε_f. Remarkably, Poisson's ratio v does not differ significantly between the dry and the wet state, but a pronounced difference is present for the two observation directions of the samples which were tested in transverse direction. While for the observation direction I the values for v amount to 0.29 in the dry state and 0.28 in the wet state, the corresponding values decrease to 0.08 in both states for the observation direction II. Table 1 summarizes the characteristic data from the compression tests of all samples from both lobsters.

While the samples tested in normal direction fractured by cleavage induced by cracks along the normal direction, 16 out of 24 samples tested in transverse direction show a well defined fracture plane oriented 45° to the compression direction and perpendicular to the cuticle surface (Fig. 11d).

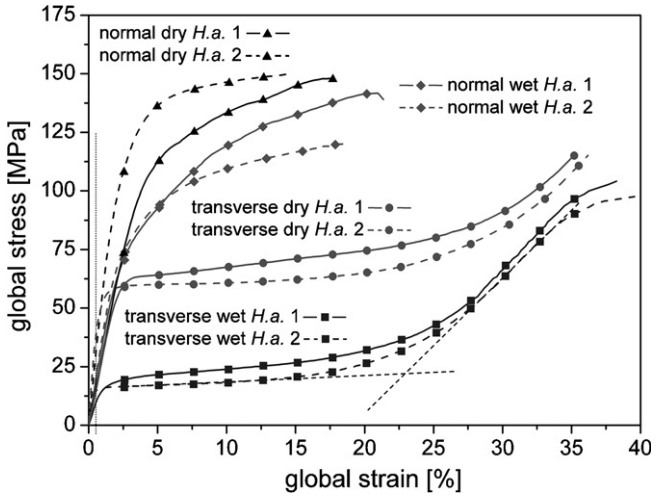

Fig. 5. Compression tests of mineralized endocuticle from two different *Homarus americanus* specimen (*H.a.*1, *H.a.*2). The graph depicts the global averaged stress–strain behavior under compression of the endocuticle obtained in normal and transverse direction (see Fig. 3) both in dry and in wet state. The interception points of the dashed straights fitted to the curves obtained for compression in transverse direction give the values for strain (ε_d) and stress (σ_d) at densification. The vertical dotted line indicates the strain range used for determining Poisson's ratio (v) and structural stiffness (s_{st}).

3.2. Shear tests

Shear tests were performed on dry samples in order to determine differences in the fracture energy under shear loading for different shear planes and directions. In Fig. 6, the stress–displacement curves for the three different shear modes are shown. The area under the averaged curves corresponds to the fracture energy. The obtained values of fracture energy in descending order are 4740 J/mm^2 for shear mode II, 4400 J/mm^2 for shear mode I, and 2800 J/mm^2 for shear mode III.

3.3. Strain analysis

3.3.1. Strain maps

In order to investigate the strain evolution under compression not only at a global but also at a local microscale, strain mappings were created using the digital image correlation (DIC) method. This was done by computing the displacement gradient tensor from data obtained from the distortion of the gray scale pattern in the previously defined areas of interest on the surface of all samples during compression. Subsequently, the strain tensor was derived for each deformation stage and displayed as strain ε_y in longitudinal direction (Fig. 7a) and as ε_x in lateral direction (Fig. 7b). For every tested sample orientation (normal, transverse I and II) in both states (dry and wet) a representative set of strain maps with increasing global (engineering) strain ε_g is shown in Fig. 7. The selected global strain levels are 1.0%, 5.0%, 10.0%, 20.0%, and 30.0%.

The samples tested in normal direction show a homogeneous strain pattern in both the longitudinal and the lateral direction at the beginning (Fig. 7a and b). With increasing

Table 1
Averaged mechanical properties of mineralized endocuticle from two different lobster specimens derived from compression tests

Direction	s_{st} [GPa]	ν [—]	ε_y [%]	σ_y [MPa]	ε_d [%]	σ_d [MPa]	ε_f [%]	σ_f [MPa]
Normal dry	4.7 (1.6)	0.13 (0.01)	2.4 (0.7)	96.8 (16.0)	—	—	18.7 (5.5)	147.5 (39.3)
Normal wet	4.1 (1.4)	0.10 (0.03)	1.8 (0.6)	56.4 (25.6)	—	—	19.4 (3.5)	124.7 (53.8)
Transverse dry observation direction I/II	4.6 (1.6)	0.29/0.08 (0.02/0.03)	1.6 (0.7)	54.9 (12.3)	30.2 (3.4)	87.0 (12.3)	42.3 (2.6)	163.4 (14.7)
Transverse wet observation direction I/II	3.0 (1.3)	0.28/0.08 (0.08/0.02)	0.7 (0.3)	14.0 (4.0)	24.6 (2.6)	35.1 (6.7)	35.6 (3.7)	93.4 (5.4)

s_{st}, structural stiffness; ν, Poisson's ratio; ε_y, yield strain; σ_y, yield stress; ε_d, strain at densification; σ_d, stress at densification; ε_f, strain to fracture; σ_f, stress to fracture. The standard deviations are given in brackets. A set of six samples were tested in normal and 12 samples in transverse direction both in dry and in wet state.

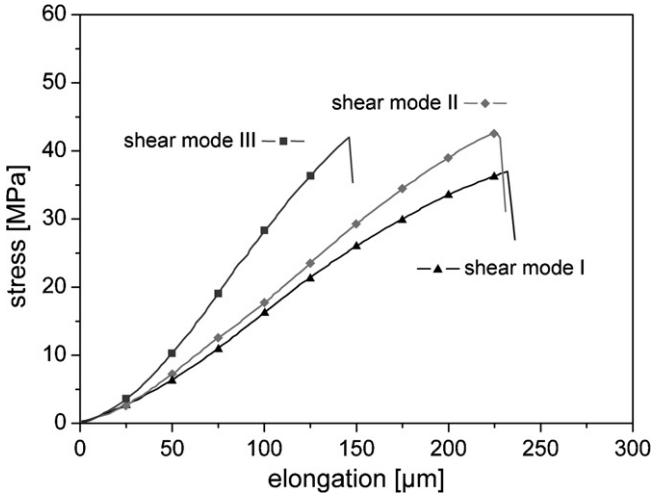

Fig. 6. Averaged displacement–stress curves for the three different shear modes I, II, and III.

global strain, zones of elevated strain ε_y appear on both ends of the samples in the longitudinal direction. In the samples tested in the wet state band shaped areas of elevated strain ε_x form which are oriented parallel to the compression direction and indicate preferred regions where cracks evolved before failure (Fig. 7b).

The samples tested in transverse direction show band shaped zones of high local strain in longitudinal direction which expand in the adjacent relatively undeformed areas during deformation. While in the corresponding areas in lateral direction these zones of high local strain are also visible in the observation direction I, the strain ε_x remains at relatively low level in observation direction II. Significant differences between the dry and the wet state cannot be seen.

3.3.2. Strain profiles

For a quantitative local strain analysis, one section was defined along the longitudinal axis and another one along the lateral axis in the center of each sample (Fig. 7). The ten curves in every diagram display the evolution of the strain profiles at each level of global (engineering) strain ε_g for each testing and observation direction in the dry and in the wet state. In the upper row of diagrams the strain profiles show the distribution of the strain in longitudinal direction ε_y along the compression direction in the center of the test specimen. In the lower row of diagrams the strain profiles show the distribution of the strain in lateral direction ε_x perpendicular to the compression direction in the center of the test specimen (Fig. 8).

The strain profiles of the samples tested in normal direction reflect the homogeneous strain evolution in the longitudinal direction ε_y and in the lateral direction ε_x with increasing global strain as seen in the corresponding strain maps. In the diagram showing the strain evolution in transverse direction, observation direction I a strong gradient in strain profile in the longitudinal direction ε_y can be seen at global strains ε_g between 5% and 10% compared to the one of the lateral direction ε_x. In observation direction II a similar strain evolution can be observed, however, the strain in the lateral direction ε_x increases less strongly than in the observation direction I.

3.4. Microstructure of cuticle after compression testing

After the compression tests the microstructure of the samples was investigated using scanning electron microscopy. The fracture surfaces of the cleaved samples are shown in Figs. 9 and 10. The samples tested in the normal direction achieved a deformation of about 10% without showing significant damage to the microstructure. Also at higher strains signs of deformation cannot be observed due to the complex microstructure and fracture surface (Fig. 9).

In the samples tested in transverse direction both in the dry and in the wet state two characteristic deformation patterns are visible which depend on the orientation of the chitin–protein fibers with respect to the compression direction (Fig. 10). In the layers where the fibers are oriented perpendicular to the compression direction the pore canals are collapsed and microcracks have formed in the dry (Fig. 10b), but not in the wet state (Fig. 10e). In contrast, in the layers where the fibers are oriented parallel to the compression direction the fiber bundles have buckled irregularly into the cavities of the pore canals (Fig. 10c and f).

4. Discussion

Biological materials like arthropod cuticle perform highly efficient with respect to their boundary conditions.

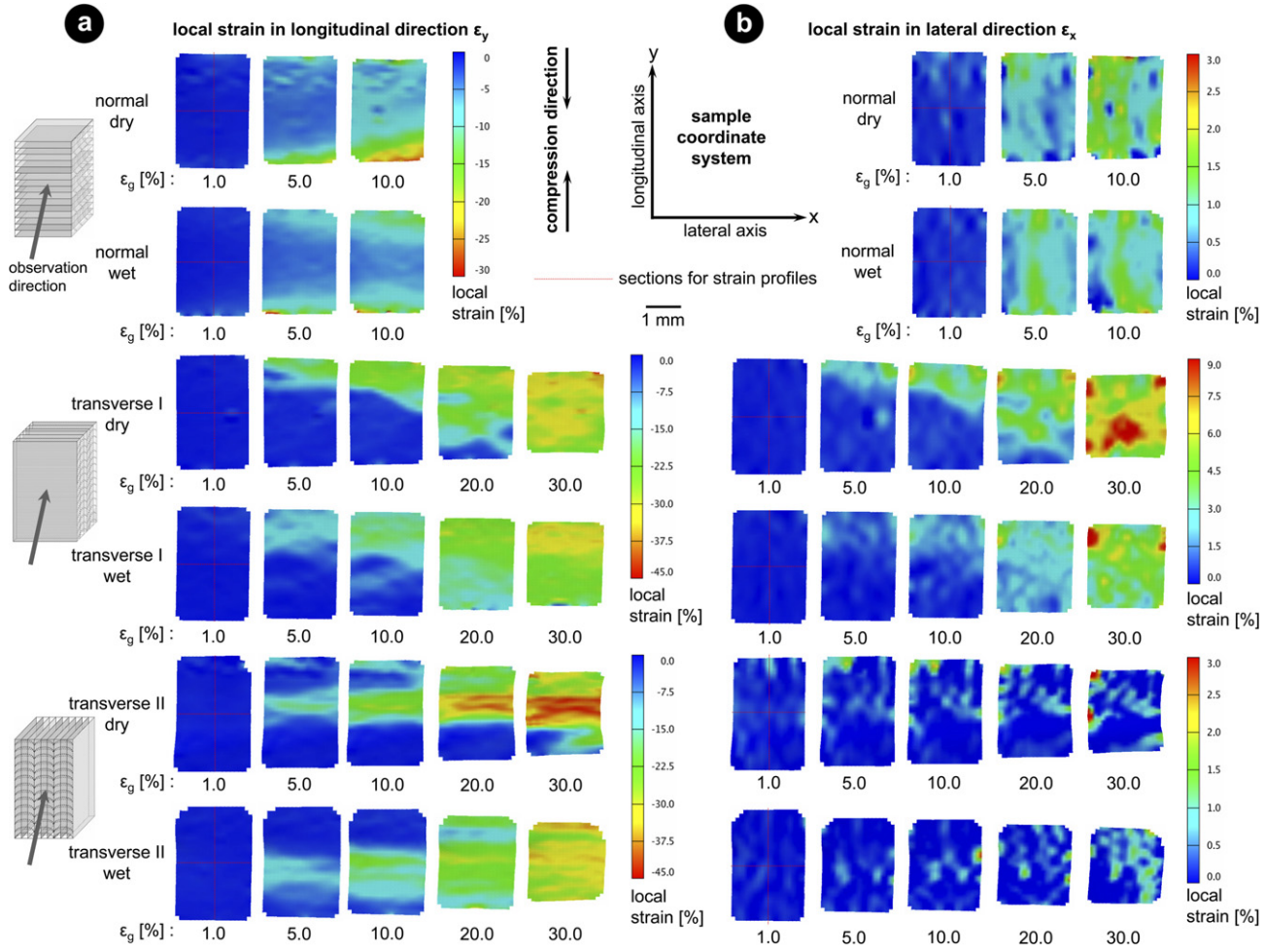

Fig. 7. Strain maps showing the strain evolution under compression in normal and in transverse direction for increasing global strain ε_g in the dry and the wet state. The local strain is displayed as ε_y in longitudinal direction (a) and as ε_x in lateral direction (b). The thin red lines drawn in the maps in (a) and (b) indicate the position of the sections used to create the strain profiles.

The selection of components used by nature is driven by their availability and the energy which is required to synthesize them (Elices, 2000). The major components in most crustacean cuticles are chitin, proteins, and minerals. By merging these components into a multiscale hierarchical composite material, each component contributes differently to the overall mechanical properties depending on its fraction, size, arrangement, and interface properties. The chitin nanofibrils are stiff in their longitudinal axis which is identical to the chitin molecule backbone established by covalent bonds, while the hydrogen bonds prevailing in the transverse directions lead to lower stiffness values (Nishino et al., 1999; Xu et al., 1994). The protein matrix can deform plastically and the mineral particles can be considered as hard and tough as their size is about a few nanometers (Gao et al., 2003). In the exoskeleton of the lobster, the overall properties of a functional unit like a claw are determined by its geometry (shape, thickness) and the local mechanical properties of the cuticle. The properties at specific locations are modulated by modifications in microstructure and are adjusted to withstand the occurring local stresses (Wegst and Ashby, 2004). This explains the variance of the obtained values in samples from different locations in one claw as well as differences in properties between different individuals (Fig. 5 and Table 1). The resulting mechanical properties of biological materials are comparable to those of man-made materials and have been summarized in material properties charts of specific properties like the ratio of stiffness and density (Wegst and Ashby, 2004).

Due to the sophisticated arrangement of the components which is exemplified in the hierarchical organization found in many biological materials like plywood and honeycomb-like structures in the lobster cuticle, these materials show anisotropy at different length scales. This anisotropy can change from one level to another. The chitin crystals in the nanofibrils which have a strong *intrinsic* anisotropy in their stiffness (Friak et al., personal communication) generate anisotropy in the mineralized chitin fibers which already represent a nano-composite. The planes of mineralized chitin fibers which build up the twisted plywood structure in the lobster cuticle are laminates which are similar to unidirectional reinforced fiber composites (Piggott, 1980). By superimposing these planes the anisotropy is cleared

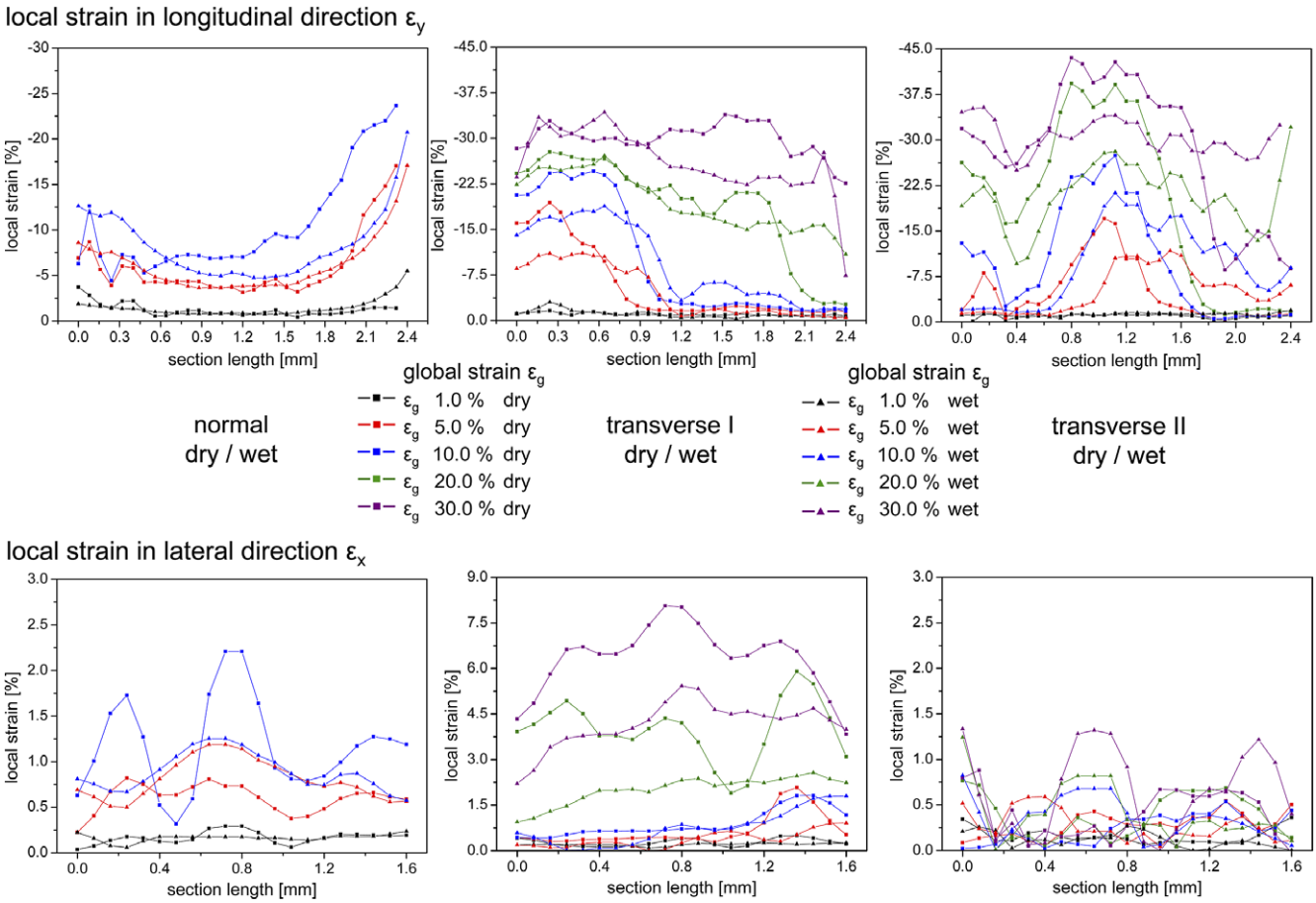

Fig. 8. Strain profiles showing the local strain evolution of ε_y in the longitudinal direction and of ε_x in lateral direction both in the dry and the wet state. Each curve displays the development of the local strain along the sections in longitudinal or in lateral direction at a distinct global strain ε_g as marked in the corresponding strain map (Fig. 7a and b).

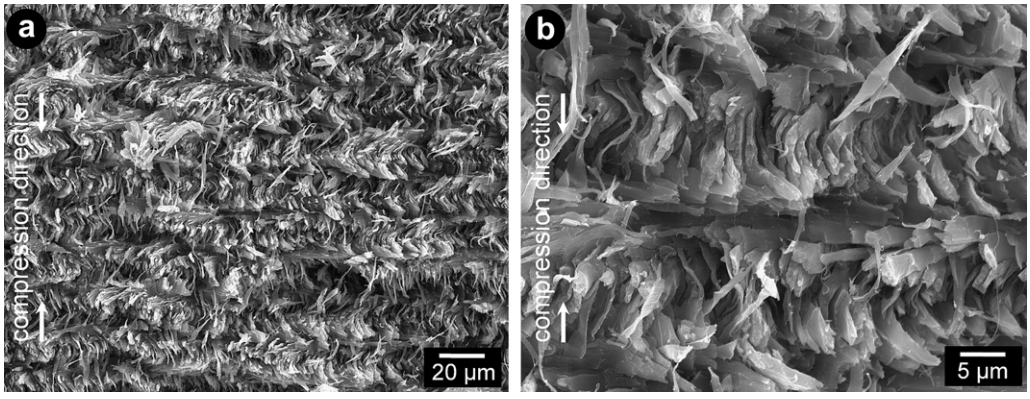

Fig. 9. SEM micrographs of compression test specimens fractured after being tested in normal direction in the dry state. (a) The samples achieved a deformation of about 10%, significant damage to the microstructure cannot be observed, even at higher resolutions (b).

but on this level a new, more structurally based anisotropy arises from the honeycomb-like structure of the material.

Under compression the endocuticle of the American lobster displays a strong structural anisotropy in the global stress–strain behavior. While the samples which were tested in normal direction show a large linear elastic region and an onset of plasticity, the samples which were tested in transverse direction show an extended plateau region after a relatively small elastic region and at the end a steeply rising portion of the stress–strain curve. In the dry state the structural stiffness in the normal direction and in transverse direction are almost equal (Table 1). In the wet state the structural stiffness in normal direction is higher than in transverse direction and only slightly lower than the value

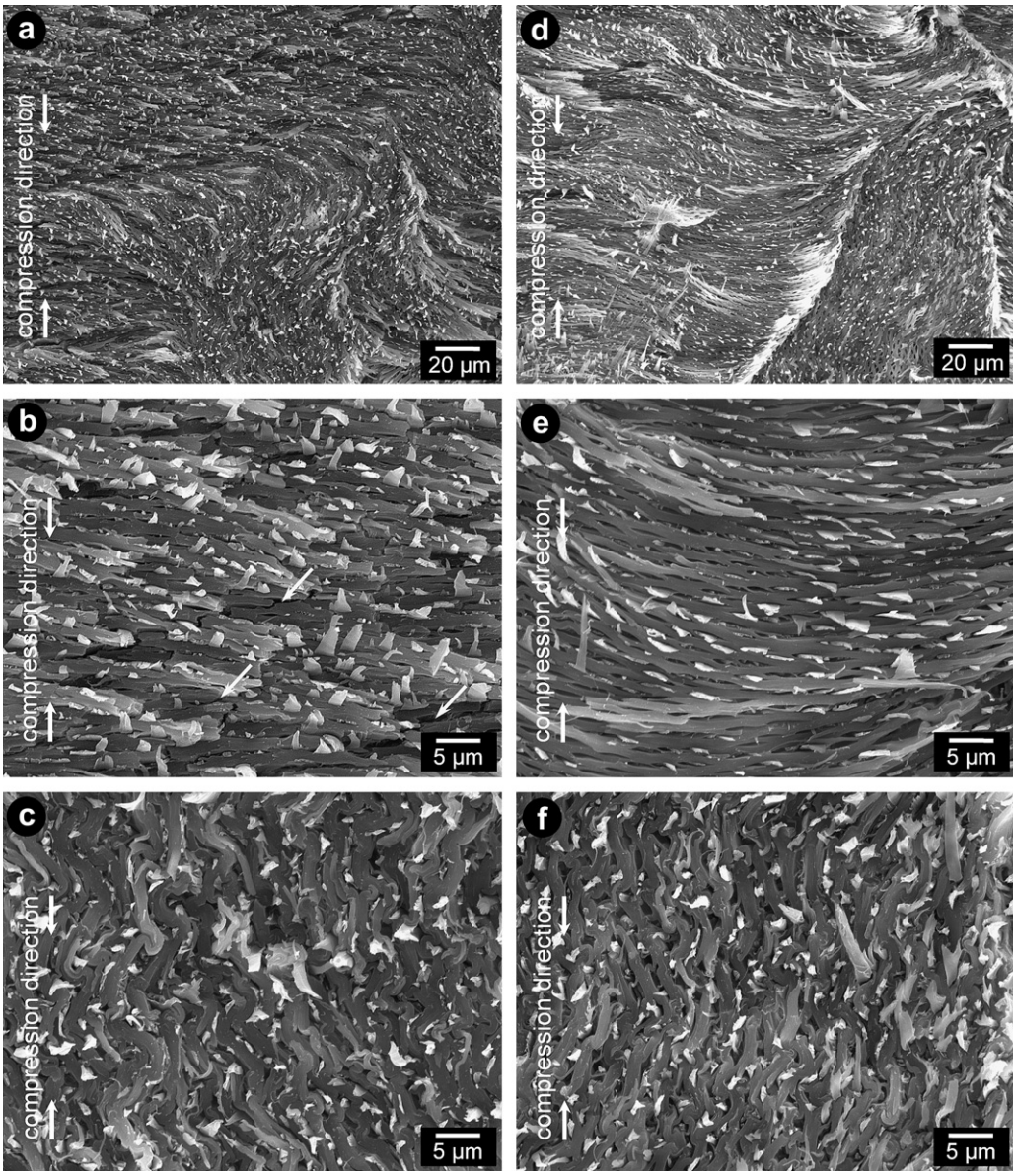

Fig. 10. SEM micrographs of compression test specimens fractured after being tested in transverse direction in the dry state (a–c) and in the wet state (d–f). (a) Overview of the fracture surface of a dry sample tested in transverse direction. (b) In layers where the fibers are oriented perpendicular to the compression direction the pore canals are collapsed and microcracks (arrows) have formed. (c) In layers where the fibers are oriented parallel to the compression direction the fiber bundles have buckled irregularly into the cavities of the pore canals. (d) Overview of the fracture surface of a wet sample tested in transverse direction. (e) In layers where the fibers are oriented perpendicular to the compression direction the pore canals are collapsed, but no microcracks are visible. (f) In layers where the fibers are oriented parallel to the compression direction the fiber bundles have buckled irregularly into the cavities of the pore canals.

obtained for the dry samples (Table 1). Apparently, dehydration shows only little effect on the structural stiffness in normal direction, while in transverse direction the structural stiffness increases by a factor of 1.5 from the wet to the dry state. The effect of dehydration on the Poisson's ratio is small in both compression directions. Noteworthy is the difference in Poisson's ratio between observation directions I and II of transversely compressed samples. Both in dry and in wet state, Poisson's ratio is about the factor 3.6 higher for the observation direction I than for the observation direction II. Compared to Poisson's ratios obtained in tensile tests that amounted to about 0.33 in the dry and in the wet state, the values for observation direction I are slightly lower (Sachs et al., 2006a). It is remarkable that when compressed in transverse direction, the elastic deformation in the normal direction of the cuticle is much smaller than in the transverse direction of the cuticle. This behavior can be explained as an effect of the honeycomb-like structure of the pore canal system and the direction of the applied stress. When the cuticle is loaded in transverse direction, the pore canals are compressed and broaden in transverse direction, which corresponds to the cross section of the pore canals. In normal direction, which corresponds to the long axis of the pore canals, the

increase in length during compression is negligible (Fig. 11b and c). The deformation behavior is illustrated schematically in Fig. 11.

The beginning of the plastic deformation is defined by the yield strain and stress. The yield strain amounts to higher values in the normal direction than in the transverse direction and increases from the wet to the dry state. The same trends can be observed for the yield stress which is in both the dry and the wet state higher in normal direction than in transverse direction. In normal direction the difference in the yield strain and stress is less pronounced between the dry and the wet state while in transverse direction desiccation has a slightly higher effect on the values of the yield strain and yield stress. In contrast to the normal direction the yield point marks the beginning of the plateau region in the transverse direction. After reaching a critical stress level the structure deforms continuously without a strong increase in stress. This deformation behavior is similar in the dry and the wet state but the stress is shifted to much higher values in the dry state. Considering the honeycomb-like structure, the observed stress values are the threshold at which the pore canals probably start collapsing. A similar behavior has been described for polycarbonate honeycombs (Papka and Kyriakides, 1998). After the densification which is reached at a strain of about 30% and a stress of 87 MPa in the dry state and of 25% and 35 MPa in the wet state, the stress increases stronger in the dry state than in the wet state. The final strain to fracture and stress to fracture values are higher for dry cuticle than for wet cuticle. In normal direction the strains to fracture are much lower compared to the transverse direction, whereas the corresponding stresses to fracture are higher for wet but lower for dry cuticle.

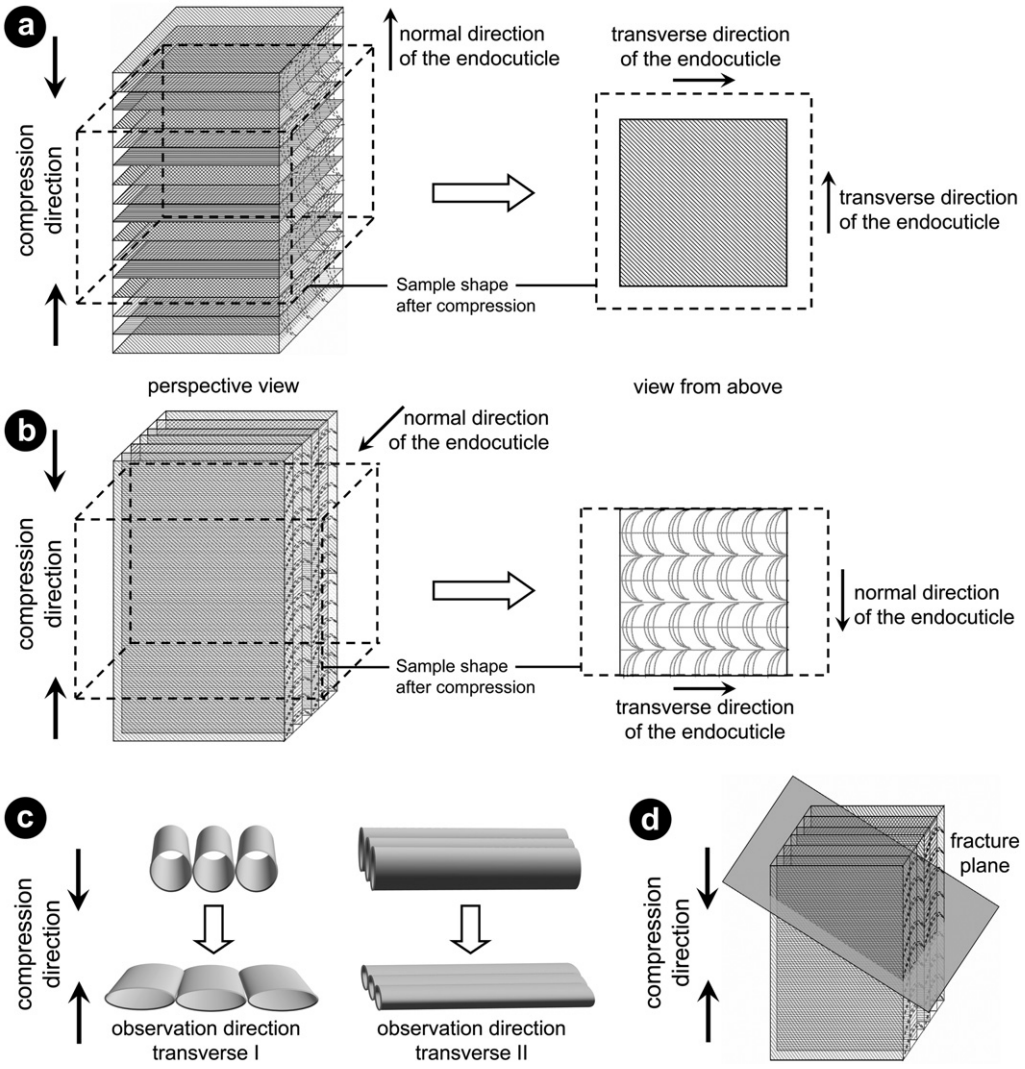

Fig. 11. Schematic illustration of the elastic–plastic deformation of the endocuticle under compression in the normal direction (a) and in the transverse direction (b) of the endocuticle. The dashed lines mark the shape of the specimens after deformation. (c) Schematic depiction of the deformation of pore canals compressed in transverse direction. When observing the cuticle surface (transverse I), lateral broadening caused by collapsing pore canals is visible. During observation of the cuticle's cross section (transverse II) this broadening is also occurring, but does not become visible. (d) Schematic showing the orientation of the fracture plane in samples tested in transverse direction.

A fundamental difference was observed in the failure of the samples. While the samples tested in normal direction failed by cleavage in compression direction, the samples tested in transverse direction showed a distinct fracture plane oriented perpendicular to the cuticle surface and 45° to the compression direction (Fig. 11d), which is equal to the direction of the maximum shear stress. This can be explained by failure of the structure along the long axes of the pore canals, resulting in the propagation of the crack from one pore canal to the next. To investigate the origin of these phenomena shear tests were performed on dry cuticle to evaluate the fracture energy which is needed to create distinct fracture planes. In the twisted plywood structure of the cuticle, two different shear planes exist which are oriented either parallel to the cuticle surface (mode I) or perpendicular to the cuticle surface (modes II and III). The difference between mode II and III is the shear direction which in this case can be in normal or in transverse direction of the cuticle (Fig. 4b and c). A fracture of mode II has the highest fracture energy because the planes of mineralized fibers are displaced against each other longitudinally with respect to cuticle geometry and the fibers have to be fractured. In mode I the fracture leads to delamination of the superimposed mineralized fiber planes and lateral movement. Additionally, the pore canal tubes are sheared off. The fracture energy amounts to slightly lower values than mode II. In mode III the fracture energy is reduced about 40%. In this case neither the pore canals nor the mineralized fiber planes have to be sheared off. In a unidirectional fiber reinforced composite the fracture plane is also oriented 45° to the compression direction and parallel to the fiber axis if the composite is loaded perpendicular to the fiber orientation (Piggott, 1980). The numerous pore canal tubes may play an important role as they act like the unidirectional fibers in this load case and likely stitch the mineralized fiber planes together improving the resistance against delamination (Dow and Dexter, 1997). Presumably, in crustaceans the original function of the pore canal system is the transport of minerals used for hardening the new exoskeleton after the molt (Dillaman et al., 2005). Our data suggest that the pore canal system also performs structural functions in the lobster's exoskeleton. Moreover, previous studies have shown that the pore canal tubes also contain chitin fibers, which are probably reinforcing them (Raabe et al., 2006). The local strain analysis revealed significant differences in the plastic deformation behavior between samples which were compressed in normal and in transverse direction. By comparing the two observation directions in the transversally compressed cuticle, a strong anisotropy in the plastic deformation can be found. While in the samples tested in normal direction a relatively homogeneous strain distribution was observed in longitudinal direction, the samples tested in transverse direction developed band-like regions of high strain which expanded into the adjacent areas (Fig. 7a). Their evolution corresponds to the plateau region in the global stress–stain curve indicating that in these zones the honeycomb-like structure of the pore canal system is already collapsed while the adjacent areas are still intact. The fact that they appear at different positions in the displayed specimens could be due to local variations in microstructure like different mineral content, causing the structure to start collapsing in the weakest spot of the respective sample. Remarkably, similar zones are only visible in observation direction I for the local strain in lateral direction while in observation direction II the local strain remains at a very low level. These differences in the level of lateral strain appear both in wet and in dry state and can be explained as effect of the microstructure and the direction of the applied stress, analogously to the elastic behavior of the samples described above. During compression in transverse direction the samples become shorter in longitudinal direction due to collapsing pore canals which are responsible for the honeycomb-like structure. In lateral direction two deformation modes are observed depending whether one looks at the surface of the sample (transverse I) or at the cross section of the sample (transverse II). In transverse I the collapsing pore canals lead to a broadening of the sample which becomes visible as elevated lateral strain. This broadening of the sample cannot be observed in transverse II because the collapsing pore canals are not elongated. From this perspective the broadening is out of the image plane and only leads to a movement of the sample surface towards the observer (Fig. 11b and c). Distinct differences of the local deformation cannot be observed between the dry and the wet state. The strain profiles further support the proposed mechanism. Tensile tests combined with DIC performed on *H. americanus* endocuticle from the same morphological locations have shown heterogeneous strain patterns with evenly distributed domains of low and elevated local strain which have been attributed to inhomogeneities of the microstructure like cuticular pores (Sachs et al., 2006a). Due to the larger global strain intervals necessary for the experimental approach in this study, comparable patterns of local strain could not be observed. The compression tests do not provide new evidence that could better explain the former findings.

The underlying deformation mechanisms become visible by examining the microstructure of test specimens after compression. Due to the complex microstructure, it is difficult to identify signs of deformation in the samples tested in normal direction in the dry and the wet state, as they were merely deformed about 10% (Fig. 9). In contrast, in the transverse testing direction two forms of deformation mechanisms can be observed. In the layers where the fibers are oriented perpendicular to the compression direction the pore canals are collapsed (Fig. 10b and e) while in the layers where the fibers are oriented parallel to the compression direction the fiber bundles buckle into the cavities of the pore

canals (Fig. 10c and f). Noteworthy, the pore canal tubes appear hardly damaged and are obviously able to prevent delamination of the layers when the layers are distorted against each other. Consequently, the samples do not expand in this direction (Fig. 10b) as visible for the observation direction II in the strain maps (Fig. 7b). The buckling of fibers demonstrates their ability to undergo large plastic deformation in the wet but also in the dry state. However, in the dry state microcracks are visible which do not lead to a brittle failure due to the compression loading. The described deformation is likely to take place in the plateau region of the stress–strain curve. When a critical stress level is reached in transverse direction, the honeycomb-like structure starts to collapse as observed by the appearance of bands of high strain in the strain maps (Fig. 7a and b). Progressively, the adjacent structure fails which can be seen as expansion of the zones of high deformation in the strain maps. There is no significant difference in the deformation behavior in transverse direction in the dry and the wet state except that the stress threshold is much higher in the dry than in the wet state. During compression, hydration does not seem to affect the deformation and fracture behavior of lobster cuticle in such a dramatic way than during tension (Sachs et al., 2006a). This is due to the fact that beyond the yield point the endocuticle undergoes a densification instead of a separation of fibers. This hinders crack opening and propagation and thus delays the failure of the test specimens. Nevertheless, hydrated samples are more ductile and support higher strains to fracture than dry samples. Additionally, hydration seems to impede the formation of microcracks in the structure during compression, which supports the role of water as a plastifier (Vincent and Wegst, 2004).

Generally, the observed characteristics in the deformation are typical for honeycombs. The observed and measured properties in transverse direction of lobster endocuticle are quite similar to the mechanical response of a classical honeycomb in its in-plane direction. The same is valid for the normal direction which corresponds to the out-of-plane direction of a honeycomb structure (Gibson and Ashby, 1997).

5. Conclusions

The cuticle of the American lobster *H. americanus* displays a pronounced anisotropy when mechanical loads are applied from different directions with respect to its microstructure. The compression tests reveal that the material deforms similar to a honeycomb structure. When tested in normal direction of the cuticle (out-of-plane) the material shows an onset of plasticity at a high level of stress before it fails. When tested in transverse direction (in-plane), the samples display an extended plateau region during which the microstructure collapses followed by further densification. The strain maps and profiles show that the geometry of the samples tested in transverse direction changes only in the direction perpendicular to the pore canals. The observed broadening is caused by the collapse of the pore canal system's cavities. Whether the structure is dry or still hydrated seems to play only an insignificant role on the deformation behavior but affects the required forces. It is noteworthy that the fracture plane in samples tested in transverse direction is oriented 45° to the compression direction and that the structure fails along the long axis of the pore canals. The shear tests confirm that this mode of fracture requires much less energy than any alternative possibilities.

References

Andersen, S.O., 1999. Exoskeletal proteins from the crab *Cancer pagurus*. Comp. Biochem. Physiol. A 123, 203–211.

Bouligand, Y., 1970. Aspects ultrastructuraux de la calcification chez les Crabes. In: 7e Congrès int. Microsc. Électr., Grenoble, France, t. 3, pp. 105–106.

Compère, P., Goffinet, G., 1987. Ultrastructural shape and 3-dimensional organization of the intracuticular canal system in the mineralized cuticle of the green crab *Carcinus maenas*. Tissue Cell 19, 839–857.

Dillaman, R.M., Hequembourg, S., Gay, M., 2005. Early pattern of calcification in the dorsal carapace of the Blue Crab, *Callinectes sapidus*. J. Morphol. 263, 356–374.

Dow, M.B., Dexter, H.B., 1997. Development of Stitched, Braided and Woven Composite Structures in the ACT Program and at Langley Research Center (1985 to 1997) Summary and Bibliography. NASA CASI (301) 621-0390.

Elices, M., 2000. Structural Biological Materials: Design and Structure–Property Relationships. Pergamon, New York.

Factor, J.R., 1995. Introduction, anatomy and life history. In: Factor, J.R. (Ed.), Biology of the Lobster *Homarus americanus*. Academic Press, New York, pp. 1–11.

Gao, H., Ji, B., Jaeger, I.L., Arzt, E., Fratzl, P., 2003. Materials become insensitive to flaws at nanoscale: lessons from nature. Proc. Natl. Acad. Sci. USA 100, 5597.

Gibson, L.J., Ashby, M.F., 1997. Cellular Solids—Structure and Properties, Second ed. Cambridge University Press, Cambridge, UK.

Giraud-Guille, M.-M., 1984. Fine structure of the chitin–protein system in the crab cuticle. Tissue Cell 16, 75–92.

Giraud-Guille, M.-M., 1990. Chitin crystals in arthropod cuticles revealed by diffraction contrast transmission electron microscopy. J. Struct. Biol. 103, 232–240.

Giraud-Guille, M.-M., 1998. Plywood structures in nature. Curr. Opin. Solid State Mater. Sci. 3, 221–228.

GOM, Handbook for the Aramis System, Gesellschaft fuer Optische Meßtechnik mbh, Version September 2000, Braunschweig, Germany.

Hadley, N.F., 1986. The arthropod cuticle. Sci. Am. 255, 98–106.

Nishino, T., Matsui, R., Nakamae, K., 1999. Elastic modulus of the crystalline regions of chitin and chitosan. J. Polym. Sci. B Polym. Phys. 37, 1191–1196.

Papka, D.S., Kyriakides, S., 1998. In-plane crushing of a polycarbonate honeycomb. Int. J. Solid Struct. 35, 239–267.

Piggott, M.R., 1980. Load Bearing Fibre Composites, Second ed. Kluwer Academic Publishers, Norwell, USA.

Raabe, D., Romano, P., Sachs, C., Fabritius, H., Al-Sawalmih, A., Yi, S.B., Servos, G., Hartwig, H.G., 2006. Microstructure and crystallographic texture of the chitin–protein network in the biological composite material of the exoskeleton of the lobster *Homarus americanus*. Mater. Sci. Eng. A 421, 143–153.

Roer, R.D., Dillaman, R.M., 1984. The structure and calcification of the crustacean cuticle. Am. Zool. 24, 893–909.

Sachs, C., Fabritius, H., Raabe, D., 2006a. Experimental investigation of the elastic–plastic deformation behavior of mineralized cuticle by digital image correlation. J. Struct. Biol. 155, 409–425.

Sachs, C., Fabritius, H., Raabe, D., 2006b. Hardness and elastic properties of dehydrated cuticle from the lobster *Homarus americanus* obtained by nanoindentation. J. Mater. Res. 21, 1987–1995.

Travis, D.F., 1963. Structural features of mineralization from tissue to macromolecular levels of organization in the Decapod Crustacea. Ann. NY Acad. Sci. 109, 177–245.

Vernberg, F.J., Vernberg, W.B. (Eds.), 1983. The Biology of Crustacea. Academic Press, New York, USA.

Vincent, J.F.V., Wegst, U.G.K., 2004. Design and mechanical properties of insect cuticle. Arthropod Struct. Dev. 33, 187–199.

Wegst, U.G.K., Ashby, M.F., 2004. The mechanical efficiency of natural materials. Philos. Mag. 84, 2167–2181.

Weiner, S., Addadi, L., 1997. Design strategies in mineralized biological materials. J. Mater. Chem. 7, 689–702.

Xu, W., Mulhern, P.J., Blackford, B.L., Jericho, M.H., Templeton, I., 1994. A new force microscopy technique for the measurement of the elastic properties of biological materials. Scan. Microsc. 8, 499–506.